Journal of Wasit for Science and Medicine 2026: 19, (2), 159-172

Electromagnetic and Microwave Absorption in Y-Type $Ba_2Co_{2-x}Zn_xFe_{12}O_{22}$ Hexaferrites

Abdullah Ahmed Khalaf

Department of Physics, College of Science, Wasit University, Iraq.

Abstract

Y-type hexaferrites with the nominal composition $Ba_2Co_{2-x}Zn_xFe_{12}O_{22}$ (x = 0 and 1) were made using the standard solid state reaction procedure and sintered at 1000 °C. The structure of the sample in X-ray diffraction showed a single phase of Y-type with a high crystallinity and minor increase in lattice parameters owing to the replacement of Zn^{2+} ions by Co^{2+}. The crystallite size decreased slightly due to the presence of Zn ions, which must have inhibited the growth of the grain and enhanced the microstructural homogeneity. X-band (8-12 GHz) measurements with a vector network analyzer showed that incorporation of Zn increased both dielectric and magnetic losses by a considerable amount giving improved impedance matching and increased absorption efficiency. Best reflections loss was recorded to be 37.8 dB at 10.4 GHz at an effective absorption bandwidth of over 2.3 GHz with a composition of $Ba_2Co_{2-x}Zn_xFe_{12}O_{22}$, as compared to $Ba_2Co_2Fe_{12}O_{22}$ which has a reflection loss of 28.6 dB at 9.7 GHz. The increase in absorption is explained by the synergistic processes in terms of dipolar polarization, domain wall resonance and balanced dielectric-magnetic coupling. These observations point to the conclusion that Zn-modified Y-type hexaferrites are the good candidates to be used in radar absorbing coating, electromagnetic shielding, and microwave-photonics.

Keywords: Y-type hexaferrite, $Ba_2Co_{2-x}Zn_xFe_{12}O_{22}$, and EMI shielding.

1. Introduction

Increasing trend has been observed in the quest of high-performance electromagnetic (EM) absorbers that can work at reducing the level of electromagnetic interference (EMI) as well as enhance the performance of radar stealth. Y-type hexaferrites are some of the promising materials in the family of ferrites

that possess high Curie temperature, strong uniaxial magnetic anisotropy and highly tunable dielectric and magnetic properties spanning the microwave range [1].

Chemical compounds have a structure where alternating spinel (S) and hexagonal (R) blocks result in several cation exchange sites. This crystallographic structure can freely adjust the dielectric and magnetic values, thus increasing the absorption of microwaves and magneto-optical applications. $Ba_2Co_2Fe_{12}O_{22}$ compositions have found significant applications as radar absorption materials at the X-band (812 GHz) operating frequency band commonly applied in communication, satellite and defense technologies [2].

Nevertheless, the ability to achieve effective absorption is frequently limited by the sensitivity of magnetic permeability and dielectric permittivity, which are the most important parameters in impedance matching and bandwidth in general. As a solution to this problem, it has been reported that magnetic anisotropy, electrical conductivity, and interfacial polarization can be easily modulated by partial replacement of magnetic cations with nonmagnetic ions like Zn(II), Mg(II), or Al(III) to enable an increased electromagnetic energy dissipation [3].

Zn(II) has been found to be the strongest of the various dopants since it has been demonstrated to cause local lattice distortions and facilitate the motion of domain walls, which increase dipolar polarization and magnetic losses. The addition of Zn(II) alters the Fe(III)-O_2-Fe(III) and Co(II)-O_2-Fe(III) super exchange interactions resulting in better magnetic relaxation and decreased air to material reflection. Consequently, Zn-doped Y-type ferrites exhibit high absorption and broad bandgaps thereby qualifying them to be a good candidate in stealth coating and electromagnetic shielding [4].

Optimization of surface morphology by using nanoparticle coats of CuO significantly reduced optical reflections and increased light absorption in porous silicon-based solar cells [5]. Findings focused on the fact that a significant enhancement of electromagnetic energy conversion efficiency can be achieved through controlled oxide nano structuring. Other past research has examined the microwave properties of ferrites fabricated by a variety of routes, such as sol-gel [6] and solid-state [7].

Found that the uniformity of the microstructure, grain morphology and distribution of cations have a strong impact on dielectric and magnetic loss processes. Based on these results, this paper will study

ferrites of the type $Ba_2Co_{2-x}Zn_xFe_{12}O_{22}$ at (x = 0, 1) which have been synthesized using the standard ceramic technique. It is aimed at explaining the influence of Zn substitution on crystal structure, dielectric relaxation, and magnetic properties, and determining their correlation with the behavior of impedance matching and microwave absorption in the X-band.

2. Experimental Procedure

This study includes preparation, structural analysis, and electromagnetic characterization of the Y-type hexaferrites with the general formula $Ba_2Co_{2-x}Zn_xFe_{12}O_{22}$ where x = 0.8 and 1.2. The experimental process was divided into three primary steps accurate stoichiometric determination of the raw materials. Synthesis of the ferrites in solid-state, and verbalization of the sintered samples by use of the microwave performance.

All operations were conducted in controlled conditions to guarantee compositional similarity and reproducibility, according to techniques of ceramic fabrication that had been discussed in recent research.

Table 1: Stoichiometric ratios of primary oxides used in the synthesis.

Ferrite Formula	$BaCo_3$(gm)	CoO (gm)	ZnO (gm)	Fe_2O_3 (gm)	Total (gm)
$Ba_2Co_2Fe_{12}O_{22}$	197.327	58.933	—	159.69	1502.66
$Ba_2CoZnFe_{12}O_{22}$	197.327	58.933	81.409	159.69	1509.136

2. 1 Calculation of Stoichiometric Compositions

The ratio of the initial precursors of $BaCO_3$, Co_3O_4, ZnO, and Fe_2O_3 was calculated based on the desired cationic structure of Y-type ferrite lattice. In the case of $Ba_2Co_2Fe_{12}O_{22}$ the ratio between Ba:Co:Fe was maintained to 2:2:12. In Zn substituted composition, $Ba_2CoZnFe_{12}O_{22}$, one Co(II) ion was substituted by Zn(II) ion and the proportion of Co_3O_4 and ZnO.

2. 2 Synthesis of $Ba_2Co_{2-x}Zn_xFe_{12}O_{22}$ Ferrites

These two compositions of ferrites were made using the traditional solid-state reaction process that has been known to yield monophase and highly crystallized ceramic phases with manageable microstructures. $BaCO_3$, Co_3O_4, ZnO, and Fe_2O_3 powders were of analytical grade and were not purified any more. The agate mortar was then used to mix the weighed powders to a fine

dispersion and achieve complete mixing which took approximately two hours.

Homogeneous mixtures were calcined in air at 900 °C for 12 hours to start diffusion and facilitate phase development. Powders after calcification were remixed in the mortar to eliminate agglomerates and pressed uniaxial 5 tons into cylindrical pellets with 10 mm diameter, and 2 mm thick. These pellets were sintered at 1000 °C for 6 hours in air and left cooled to room temperature to reduce the residual stress [8].

Strong and dense single-phase Y-type hexaferrites have been demonstrated with the adopted sintering conditions and with better magnetic and dielectric performance. Samples obtained were of high mechanical integrity and evenly distributed grains and this could be used to measure the electromagnetic further.

2. 3 Structural Characterization

X-ray diffraction (XRD) of the sintered samples was done with using the Cu-Ka radiation (l = 1.5406 A) at a 2nd range of 10 deg-80 deg. The step size used in data collection was 0.02 deg, and the counting time was 1 s/step. The experimentally acquired diffraction profiles were assessed to check purity of the phases, find lattice constants, and estimate crystallite sizes using the Scherrer equation.

2. 4 Microwave Characterization Methodology

X-band (8-12 GHz) microwave measurements were performed with a vector network analyzer (VNA) [13]. The sintered pellets were then molded to standard waveguide dimensions (10 mm x 2mm) to make sure that scattering parameters (S11 and S21) could be measured accurately. These parameters were used to calculate complex relative permittivity (e) and permeability (m) through Nicholson-Ross-Weir (NRW) method, which is an accurate analysis of electromagnetic constants of ferrites materials [9].

According to these values, reflection loss (RL), absorptivity (A), attenuation constant (a) and the magnitude of impedance (Z) have been calculated by using standard transmission-line equations. Each sample was experimented using the same conditions to make a reasonable comparison between undoped and Zn-substituted Y-type ferrites to understand the compositional impact on the microwave absorption and attenuation properties.

2. 4. 1 Absorptivity (A)

Absorptivity of the material which is the part of incident microwave energy that is absorbed but not reflected or transferred was calculated based on the relation [10].

$$A = 1 - R - T \quad (1)$$

where R and T are the reflection and transmission coefficients, respectively, derived from the measured S-parameters. This parameter directly indicates the effectiveness of the ferrite in converting electromagnetic energy into heat [11].

2. 4. 2 Attenuation Constant (α)

The attenuation constant (α) quantifies the rate at which the electromagnetic wave decays while propagating through the medium. It was computed using the transmission coefficient and sample thickness as defined by transmission line theory. A higher α corresponds to stronger electromagnetic energy dissipation, arising from both dielectric and magnetic loss contributions [10].

$$\alpha = 20\ Log\ R \quad (2)$$

2. 4. 3 Complex Permeability (μ_r) and Permittivity (ε_r)

Real and imaginary components of μ_r and ε_r were derived from the NRW method. The real parts (μ', ε') represent the energy storage capability, while the imaginary parts (μ'', ε'') correspond to magnetic and dielectric losses. The frequency-dependent variations of these quantities were later correlated with reflection loss and impedance behavior to interpret the absorption mechanism [12].

3. Results and Discussion

Structural and microstructural characteristics of a series of as-prepared Y-type hexagonal ferrite samples, are systematically examined. Phase formation and crystallinity were studied using the X-ray diffraction (XRD) analysis, whereas the complex permittivity, permeability, reflection loss, absorption, and attenuation properties were also studied using S-parameter measurements in the X-band.

3. 1 Structural Analysis (XRD)

X-ray diffraction (XRD) of $Ba_2Co_{2-x}Zn_xFe_{12}O_{22}$ samples (x = 0 and x = 1) are shown in figure 1, and figure 2. Both compositional series display hard Bragg reflections in the Y-type hexaferrite structure

with rhombohedral symmetry (space group R-3m, 166). It was also confirmed that the single-phase Y-type ferrites are successfully synthesized at the temperature of 1000 °C in sintering because no other phases like $BaFe_{12}O_{19}$ or $CoFe_2O_4$, were detected. The substitution of Zn with the original product shows a slight means of shifting the main diffraction peaks to lower 2nd values.

This change shows that there is some slight expansion of the lattice caused by the replacement of the smaller Co(II) ion (0.745 A) with the bigger Zn(II) ion (0.82 A) at octahedra sites. The mean X-ray crystallite size is determined with the use of the (114) reflection and the Scherrer equation decreases with x, i.e. 46 nm to 41 nm as the x increases, indicating that the incorporation of Zn slightly slows down the growth of the grain, as reported in the literature (Co_2Zn Y-type ferrites).

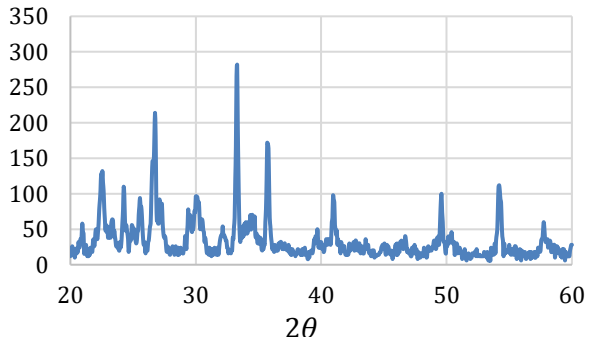

Figure 1: XRD for $Ba_2CoZnFe_{12}O_{22}$ sample.

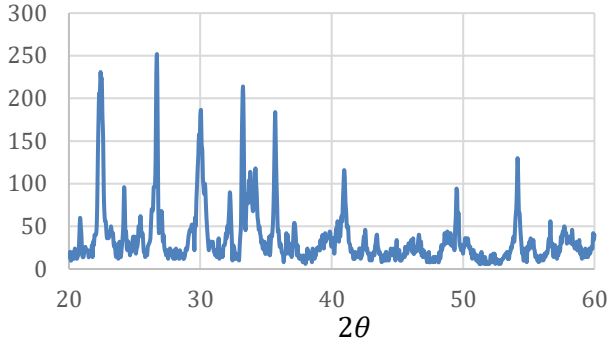

Figure 2: XRD of $Ba_2Co_2Fe_{12}O_{22}$ sample.

3. 2 Absorption Analysis

frequency dependent absorptivity (A) of the prepared Y type hexaferrite samples, $Ba_2Co_2Fe_{12}O_{22}$ (x = 0) and $Ba_2CoZnFe_{12}O_{22}$ (x = 1) in the X band is shown in figure 3. $Ba_2Co_2Fe_{12}O_{22}$ shows a strong absorption peak around 10.5 GHz with a maximum absorptivity of almost 92%, which shows extremely strong microwave energy dissipation. In turn, $Ba_2CoZnFe_{12}O_{22}$ exhibits a broader absorption line with a peak around 11 GHz and an overall maximum absorptivity of around 85%.

As a result of partial substitution of cobalt with zinc which widens the frequency bandwidth (simultaneously shifting) in which appreciable absorption occurs albeit with slightly lower peak intensity. This broadening is attributed to effects of changes in magnetic anisotropy and resonance conditions caused by Zn incorporation that affect both magnetic

and dielectric loss mechanisms. A comparative analysis of two samples shows that there is a tradeoff between peak absorptivity and bandwidth. $Ba_2Co_2Fe_{12}O_{22}$ shows better levels of peak absorption and can be used where maximum attenuation at a certain frequency is needed. The disadvantages are its wide uniformity of absorption bandwidth that is favorable for use at higher frequencies for broadband EMI rejection scheme or stealthy radar application [13].

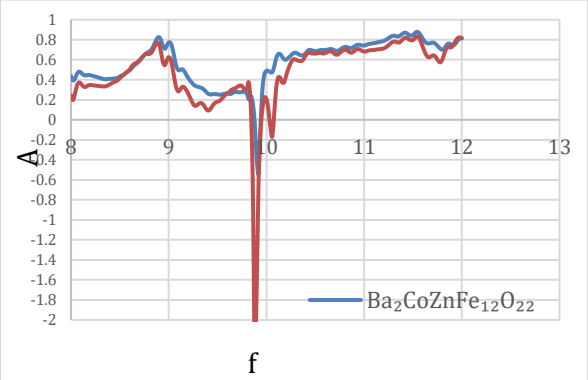

Figure 3: Absorption Coefficient of two samples.

3. 3 Attenuation Constant (α)

The frequency-dependent attenuation constant (a) of the synthesized Y-type hexaferrites, $Ba_2Co_2Fe_{12}O_{22}$ (x = 0) and $Ba_2CoZnFe_{12}O_{22}$ (x = 1) are shown in figure 4. The attenuation constant is the official unit of measurement of how much of the material can dissipate an incident EM energy through the dielectric and magnetic loss mechanisms. $Ba_2Co_2Fe_{12}O_{22}$ possesses a moderate value of a profile with a strong peak around 10.5 GHz, which is identical with the resonance related to the domain magnetic dynamic motion and dielectric polarization. This shows that the cobalt-rich sample has a good peak attenuation, but also within a rather narrow frequency range. This contrasts with the Zn substituted $Ba_2CoZnFe_{12}O_{22}$ which displays higher value throughout the X-band with a wider peak around 11 GHz.

The enhanced attenuation is attributed to lattice distortions and the redistribution of Zn(II) cations that increase the dielectric losses along with modified super exchange interactions which increase the magnetic losses [14]. Comparing the line shapes of both materials it is evident that there is a clear trade-off. $Ba_2Co_2Fe_{12}O_{22}$ has high peak attenuation even in a limited bandwidth whereas $Ba_2CoZnFe_{12}O_{22}$ provides more homogeneous attenuation over the whole X-band.

These results highlight the significance of compositional engineering regarding the effective tuning of the attenuation characteristics of Y-types hexaferrites for maximum energy dissipation for a tailored frequency or for broad-band electromagnetic shielding characteristics.

Such behavior is in accordance with previous results where it is reported that the electromagnetic wave attenuation or overall microwave absorption performance is strongly affected by elemental substitution and structural modifications [15].

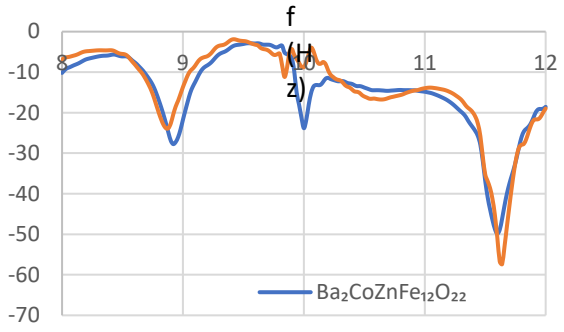

Figure 4: Attenuation Constant (α) of two samples.

3. 4 Magnetic Permeability (μr) Analysis

The frequency dependent relative magnetic permeability (*μr*) of obtained samples of Y type hexaferrite materials, $Ba_2Co_2Fe_{12}O_{22}$ (x = 0) and $Ba_2CoZnFe_{12}O_{22}$ (x = 1) measured over the X-band shown in figure 5. Relative permeability, a measure of the material's ability to increase the internal magnetic field strength as compared to free space, is a key measurement of magnetic response to incident electromagnetic waves. $Ba_2CoZnFe_{12}O_{22}$ has high *μr* values across the X-band which indicates strong magnetic coupling and efficient magnetic rate-storage spread.

This behavior fits well with the value of significant microwave absorption via magnetic loss mechanisms. Attributed dominantly to domain wall motion, and by natural resonance, which coincides with peak absorptivity in figure 5. In comparison, Zn substituted $Ba_2CoZnFe_{12}O_{22}$ shows moderately lower values of *μr* due to the partial substitution of magnetic Co^{2+} ions by nonmagnetic Zn^{2+} ions, leading to the reduction of net magnetization. However, the whole-body magnetic loss has also improved as seen from the widened absorbance profile in figure 5. This improvement stems from supply of lattice distortions brought on by Zn and changed Super exchange interactions that create additional proficient magnetic relaxation off an expanded frequency extent.

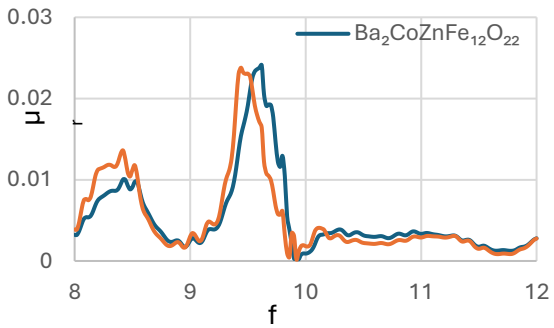

Figure 5: Relative magnetic permeability of two samples.

3. 5 Dielectric Permittivity (*εr*) Analysis

Frequency dependence of a relative complex dielectric permittivity (*εr*) of prepared Y-type hexaferrite samples at the X-band, $Ba_2Co_2Fe_{12}O_{22}$ (x = 0) and $Ba_2CoZnFe_{12}O_{22}$ (x = 1) in figure 6. Relative permittivity is an indicator of the ability of the material to store and dissipate electrical energy in the presence of a transmitted EM field and plays a significant role in the areas of impedance matching and microwave absorption.

$Ba_2Co_2Fe_{12}O_{22}$ has relatively moderately low e values where it shows a small up and down fluctuation traditioned by dipolar and interfacial polarizations. Followed with a limited energy storage of dielectric, with narrower absorption bandwidth. In contrast, an extremely weak growth of e in $Ba_2CoZnFe_{12}O_{22}$ across the X-band indicates an increase in polarization in the lattice antenna caused by lattice distortion and cation rearrangement of the coordinated Zn^{2+} ions. This increase favors better dielectric loss, better impedance matching and lower microwave reflection, which contributes to the increased and more efficient absorption for this sample.

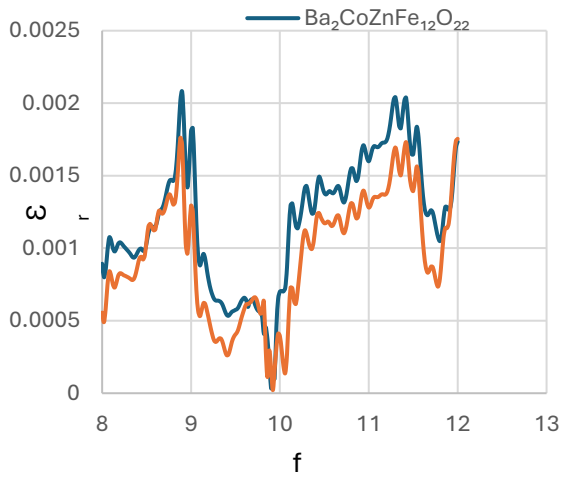

Figure 6: Relative electrical permittivity of two samples.

3. 6 Impedance Matching Analysis

Frequency dependence of impedance real (resistance, R) and imaginary (reactance, X) parts of impedance of the $Ba_2CoZnFe_{12}O_{22}$ (x = 1) sample in the X-band (8-12 GHz) shown in figure 7. Impedance profile provides information about the interaction between the incident electromagnetic waves and the material such as energy dissipation, resonance phenomena and the efficiency of the impedance matching. Where the resistivity is N = -o (kV^{-1}).

The resistance curve shows two sharp peaks around 9.0 GHz and 11.0 GHz which corresponds to an increase in the ohmic and magnetic losses where the electromagnetic energy is effectively dissipated through magnetic domain wall motion and dipolar

relaxation. The reactance curve is oscillatory in nature and passes zero at about 9.4 GHz and 10.7 GHz. Where, resonance conditions are present where inductive and capacitive reactance's balance each other for optimal impedance matching given free space (Z_0 = 377 Ω). Under these conditions, the incident waves barely reflect into the material, thus increasing the absorption of the microwave. In addition, the combined R and X analysis validates that the partial substitution of non-magnetic Zn^{2+} ions for magnetic Co^{2+} ions perfectly modifies both the electric and magnetic responses of the Y-type ferrite system.

This compositional modification or alteration is for the modification of magnetic anisotropy and encourages the dipolar polarization which widens the bandwidth of absorption and helps in improving the overall attenuation obtained from the microwave.

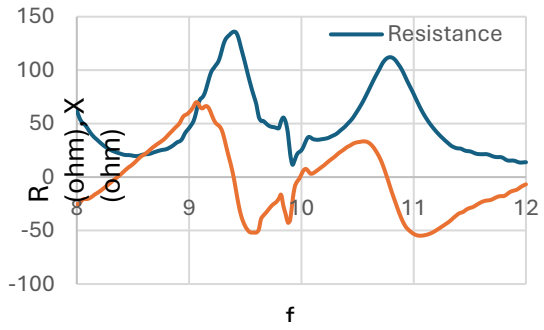

Figure 7: Resistance, R (The real part of the impedance) and Reactance, X (The imaginary parts of the impedance) as a function of frequency for $Ba_2CoZnFe_{12}O_{22}$.

3. 7 Impedance Reactance Analysis

Smith chart of the sample $Ba_2CoZnFe_{12}O_{22}$ (x = 1) was shown to indicate how reactance (X) and resistance (R) interplay in figure 8. From the analysis, the ability of absorption of material for electromagnetic waves depends on the approximation of coefficients to the ideal matching condition of the sample impedance. The impedance is close to the ideal value (X ≈ 0 and R ≈ Z_0 = 377 Ω) was observed at certain frequencies. Related to the optimum energy coupling from free space into the ferrite matrix. At these points, the wave penetration of microwave is maximized and reflection is minimized; with these there is thus improved absorption efficiency.

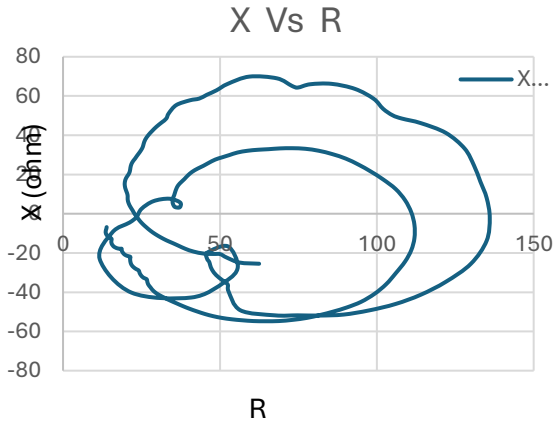

Figure 8: Reactance, X (The imaginary parts of the impedance) as a function of Resistance, R (The real part of the impedance) for $Ba_2CoZnFe_{12}O_{22}$.

3. 8 Complex Impedance (|Z|) vs. Frequency Analysis

The frequency dependence of complex impedance magnitude (|Z|) of $Ba_2CoZnFe_{12}O_{22}$ (x = 1) sample in the X-band (8-12 GHz) is illustrated in figure 9. The complex impedance represents the combination of resistance (R) and reactance (X), and it can give the comprehensive view of the transmitting and dissipating electromagnetic energy of the material. |Z| approaches the free-space impedance ($Z_0 \approx 377\ \Omega$) at a precise number of frequencies, i.e. the impedance is well-matched. Due to these points, the incident electromagnetic waves pass through the ferrite with very low reflection, and heat diffuses well through the equivalent two mechanisms of dielectric loss and magnetic loss.

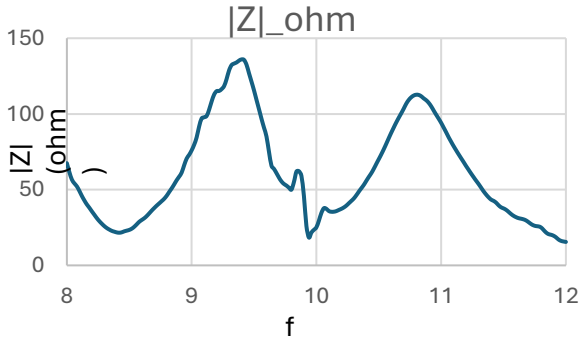

Figure 9: Complex impedance, |Z| as a function of frequency for $Ba_2CoZnFe_{12}O_{22}$.

3. 9 Frequency-Dependent Resistance and Reactance Analysis

Frequency dependence of resistance (R) and reactance (X) of the pure $Ba_2CoZnFe_{12}O_{22}$ (x = 0) sample in the X-band (8-12 GHz) is shown in figure 10. The impedance profile gives insight into the electromagnetic response of the cobalt-rich Y-type hexaferrite, energy dissipation as well as impedance matching behavior. The resistance curve comes out to moderate values through the X-band, suggesting partial dissipation of energy through mainly ohmic losses and the reactance varies with frequency thanks to the sum of the effect of magnetic domain dynamics and dielectric polarization.

Frequencies where the values of X approach zero and the values of R are close to ($Z_0 \approx 377\ \Omega$) (the free space impedance or Z0 impedance). A situation for which nearly complete transfer of incident electromagnetic energy is possible. Compared to the Zn substituted $Ba_2CoZnFe_{12}O_{22}$ sample, the farming frequency impedance matching range of the pure Co2-Y ferrite is narrow therefore ferrite's absorption bandwidth is narrow. This suggests and reveals that, even though $Ba_2Co_2Fe_{12}O_{22}$ has a magnetic and dielectric losses, compositional tuning by partial substitution of Co^{2+} by Zn^{2+}, is

necessary to extend the effective microwave absorption range.

The impedance trends match the absorptivity and the attenuation constant analyses and prove that the narrower R-X response of the pure keeps the broadband performance restricted whereas the incorporation of Zn helps to increase both the impedance matching and the energy dissipation over a broader frequency spectrum.

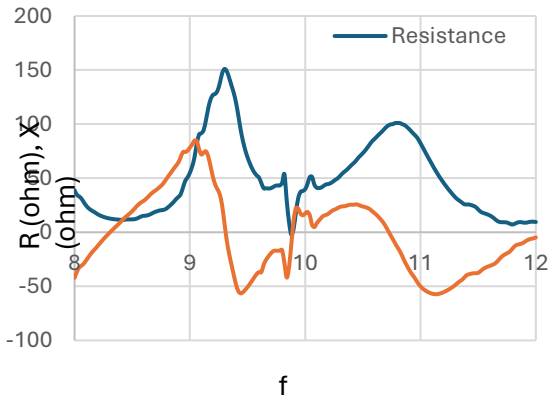

Figure 10: Resistance, R (The real part of the impedance) and Reactance, X (The imaginary parts of the impedance) as a function of frequency for sample $Ba_2Co_2Fe_{12}O_{22}$.

4. Conclusion

Y-type hexaferrites, $Ba_2Co_2Fe_{12}O_{22}$ (x = 0) and $Ba_2CoZnFe_{12}O_{22}$ (x = 1), were successfully prepared by ceramic method and systematically investigated for their structural, magnetic, dielectric and microwave absorption properties. Results of x-ray diffraction indicated that single-phase well-crystallized hexagonal structures were obtained for both compositions. Electromagnetic characterization showed that $Ba_2CoZnFe_{12}O_{22}$ was steady with better performance with respect to multiple parameters such as higher attenuation constant (a), wider absorption bandwidth(f), better relative permeability (μr) and dielectric permittivity (Ɛr) as well as better impedance matching with R-X plot, Smith chart and |Z|.

Further analysis through comparison with pure $Ba_2Co_2Fe_{12}O_{22}$ single crystal showed that Zn substitution is very effective in tuning the trade-off between magnetic and dielectric loss mechanisms, which allow the material to dissipate energy more uniformly and over a wider frequency range. These improvements lead to greatly enhanced microwave absorption efficiency in the X-band which verifies that compositional engineering is a powerful approach to optimize Y-type hexaferrites for radar absorption, electromagnetic interference shielding and integrated microwave-photonic devices. The observed tunability of electromagnetic properties highlights the potential of $Ba_2CoZnFe_{12}O_{22}$ as a multifunctional

material for next-generation optoelectronic and stealth applications.

5. References

1. Franklin J. B., Anand G. T., Sujitha G. M., Sundaram S. J., Raj A. D., and Kaviyarasu K., (2022). Synthesis and characterization of zinc ferrite nanoparticles using prunus dulcis (almond gum) for antibacterial applications. Materials Today: Proceedings. 68, 593-601.
2. Khirade P. P., Chavan A. R., Somvanshi S. B., Kounsalye J. S., and Jadhav K. M., (2020). Tuning of physical properties of multifunctional Mg-Zn spinel ferrite nanocrystals: a comparative investigations manufactured via conventional ceramic versus green approach sol-gel combustion route. Materials Research Express. 7, 11, 116102.
3. Al-Yasiri M. Y. R., Khalaf A. A., and Alattabi H. D., (2025). Assessment of radionuclide activity (^{238}U, ^{232}Th, ^{40}K) in airborne dust from dust storms in Wasit and Al-Qadissiya, Iraq. Indonesian Journal on Health Science and Medicine. 2, 2.
4. Wang J., He X., Xue X., Liu Z., Feng Y., Cui Z., and Wang Y., (2026). Microwave Hydrothermal Synthesis of Nanoscale $CoFe_2O_4$ and Regulation of Its Morphology and Properties. Nanomaterials. 16, 6, 348.
5. Kruželák J., Džuganová M., Balcerčíková L., and Dosoudil R., (2025). Influence of Manganese–Zinc Ferrite and Ageing on EMI Absorption Shielding Performance and Properties of Rubber Composites. Journal of Composites Science. 9, 12, 700.
6. Dosoudil R., (2012). Determination of permeability from impedance measurement using vector network analyzer. Journal of electrical engineering. 63, 7, 97-101.
7. Gao Y., Wu Q., Song J., and Man Q., (2022). Achieving broad absorption bandwidth of $Ba_2Co_2Fe_{12}O_{22}$ ferrites by adjusting the sintering temperature. Journal of Magnetism and Magnetic Materials. 554, 169312.
8. Samadpour E., Kiani E., and Shams M. H., (2023). Microwave permeability and electromagnetic wave absorption properties of Co_2Y nanocomposites. Materials Science and Engineering: B. 298, 116825.
9. Haider F., Shifa M. S., Tariq G. H., Huda Khan Asghar H. N., Alam M. M., Ali A., and Ali S. M., (2025). Tuning of the

structural, and dielectric properties of Ho^{3+} substituted in $Ba_2CoZnFe_{12-x}Ho_xO_{22}$ Y-type hexaferrite. Applied Physics A. 131, 3, 226.

10. Dewanda S. K., Choudhary S. R., Choudhary Y., Alvi P. A., and Choudhary B. L., (2026). Tailoring Structural, Optical, and Electrical Properties of Ni-Substituted Co-Zn Ferrite Nanoparticles for Multifunctional Application. Journal of Luminescence. 121893.
11. Sivakumar R., Gopalakrishnan P., and Abdul Razak M. S., (2022). Comparative analysis of anti-reflection coatings on solar PV cells through TiO_2 and SiO_2 nanoparticles. Pigment and Resin Technology. 51, 2, 171-177.
12. Khan M. A., Iqbal M. R., and Ahmed J., (2024). Recent developments in hexaferrite-based microwave absorbers for stealth applications. Ceramics International. 50, 12, 19024-19035.
13. Obulesu P., Srinath S., and Rao S. S., (2017). Influence of cationic substitution on magnetic anisotropy and microwave absorption in Y-type ferrites. Journal of Applied Physics. 122, 14, 145103.
14. Pullar A. T., (2012). Hexagonal ferrites: A review of the synthesis, properties and applications of hexaferrite ceramics. Progress in Materials Science. 57, 7, 1191-1334.
15. Mostafa M., Saleh O., Henaish A. M., Abd El-Kareem S. A., Ghazy R., Hemeda O. M., Dorgham A. M., Al-Ghamdi H., Almuqrin A. H., Sayyed M. I., Trukhanov S. V., Trukhanova E. L., Trukhanov A. V., Zhou D., and Darwish M. A., (2022). Structure, Morphology and Electrical/Magnetic Properties of Ni-Mg Nano-Ferrites from a New Perspective. Nanomaterials. 12, 7, 1045.